Magnetic states of Mn and Co atoms at Co_2MnGe/MgO interfaces seen via soft x-ray magnetic circular dichroism

D. Asakura, T. Koide, S. Yamamoto, K. Tsuchiya, T. Shioya, and K. Amemiya
Photon Factory, IMSS, High Energy Accelerator Research Organization, Tsukuba, Ibaraki 305-0801, Japan

V. R. Singh, T. Kataoka, Y. Yamazaki, Y. Sakamoto, and A. Fujimori
Department of Physics and Department of Complexity Science and Engineering, University of Tokyo, Bunkyo-ku, Tokyo 113-0033, Japan

T. Taira and M. Yamamoto
Division of Electronics for Infomatics, Hokkaido University, Sapporo, Hokkaido 060-0814, Japan
(Received 13 June 2010; published 15 November 2010)

The magnetic states of Mn and Co atoms in Co-rich Co_2MnGe Heusler alloy thin films facing an MgO barrier were studied by means of soft x-ray magnetic circular dichroism (XMCD). In particular, the Co_2MnGe film-thickness dependence of the Mn and Co magnetic moments was investigated. With a decrease in the Co_2MnGe film thickness to 1–2 monolayers (MLs), the spin magnetic moment of Mn decreased and the Mn $L_{2,3}$-edge x-ray absorption spectra (XAS) showed a Mn^{2+}-like multiplet structure in MnO, in contrast to samples thicker than 4 ML, indicating that the Mn atoms of the 1 and 2 ML samples were oxidized. The Co spin magnetic moment increased slightly with decreasing thickness. A Co^{2+}-like multiplet structure in CoO was not observed in all the Co $L_{2,3}$-edge XAS and XMCD, indicating that, even in the ultrathin samples, the Co atoms were not oxidized, and were more strongly spin polarized than those in the thicker samples. Co spin magnetic moments of 1.40–1.77 μ_B larger than the theoretical value for ideal stoichiometric Co_2MnGe (~ 1 μ_B) and the Co-rich film composition imply the presence of Co antisites that would lower the spin polarization.

DOI: 10.1103/PhysRevB.82.184419 PACS number(s): 75.70.−i, 68.35.Ct, 75.50.Cc, 73.20.−r

I. INTRODUCTION

Magnetic tunnel junctions (MTJs) have recently been widely studied as magnetic storage devices and magnetic sensors. To improve their performance, it is very important to understand the nature of spin-dependent conduction and develop MTJs having a high tunnel magnetoresistance (TMR) ratio with highly spin-polarized ferromagnetic electrodes. In this context, a fully epitaxial MTJ made of an MgO tunnel barrier and half-metallic ferromagnetic electrodes is very promising because the single-crystalline MgO enables coherent tunneling through the Δ_1 band that is conserving the highly polarized electron spins of the half-metallic ferromagnetic electrodes. Fully epitaxial Fe/MgO/Fe MTJs, in which Fe electrodes feature a half-metallic nature for the Δ_1 band electrons, have experimentally shown a TMR ratio of 180% (Ref. 1) at room temperature (RT) owing to coherent tunneling of the Δ_1-band electrons. This value is much higher than that in conventional MTJs consisting of polycrystalline electrodes and an amorphous AlO_x tunnel barrier.

Co-based full Heusler alloys Co_2YZ such as Co_2MnGe (CMG) and Co_2MnSi (CMS) are also promising candidates for ferromagnetic electrodes in MTJs, because some theories have predicted that they are ideal half metals.[2–5] In fact, TMR ratios of several hundred percent in Co-based full Heusler alloys with an MgO tunnel barrier have recently been reported.[6–10] Here, the TMR ratio is defined as $[\text{TMR ratio}]=(R_{AP}-R_P)/R_P$ in terms of the resistances for the parallel (R_P) and antiparallel (R_{AP}) geometries.[11] The (anti) parallel geometry means that electrode 1 is (anti) ferromagnetically coupled with electrode 2 across the thin nonmagnetic tunnel barrier. Assuming ideal half metals without interface state (Jullière's model),[12] the formula can be written as $[\text{TM Rratio}]=2P_1P_2/(1-P_1P_2)$, where P_1 and P_2 are the spin polarizations at the Fermi level (E_F) of electrodes 1 and 2, respectively.[12] In this model, if Co-based full Heusler alloys are perfectly half metallic, i.e., if P_1 and P_2 are equal to 1, the TMR ratio given by Jullière's formula[12] must be infinite. The TMR ratio of several hundred percent in real Heusler alloy/MgO MTJs implies that the half metallicity might have deteriorated for some reason.

A disorder-free X_2YZ full Heusler alloy has the $L2_1$ crystal structure having four fcc sublattices. When the elements Y and Z are randomly located, the crystal structure changes to B2. When Y, Z, and X are disordered, it changes to A2. The crystal structure change from $L2_1$ to B2 or A2 is one of the possible reasons to reduce the spin polarizations at E_F. A numerical study[13] suggests that lattice distortions and the existence of impurities at the interfaces could also reduce the spin polarization. Hence, high-quality interfaces are the key for obtaining high TMR ratios. Thus, it is very important to characterize the interfacial magnetic and electronic states of Heusler alloy/MgO MTJs.

In this study, we investigated the magnetic and electronic structures of Mn and Co atoms in CMG facing an MgO barrier using soft x-ray magnetic circular dichroism (XMCD). XMCD is an element- and orbital-selective measurement, i.e., a technique that can distinguish the Mn 3*d* electronic states from the Co 3*d* ones. We studied the CMG-film-thickness dependence of XMCD and magnetic moments of seven CMG/MgO samples with various CMG thicknesses ranging from 1 to 172 monolayers (MLs). Since it is desir-

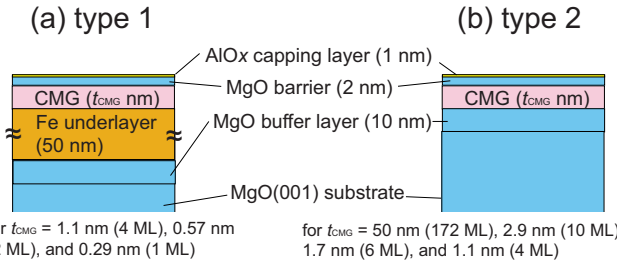

FIG. 1. (Color online) Schematic of CMG/MgO layer structure for (a) thin samples: type-1 layer and (b) thick samples: type-2 layer.

able for the electrodes in MTJs to be as thin as possible from the viewpoint of applications, it was important to investigate whether the thinner samples maintained the magnetic and electronic properties of the thicker ones. Since the XMCD probing depth was at most ≤ 5 nm,[14] the XMCD for the thinner samples predominantly reflected the interfacial magnetic and electronic states while that for thicker samples contained information about the interfacial and bulk states.

II. EXPERIMENT

A. Sample preparation and structural characterization

We prepared two types of layer structures. Ultrathin CMG films with thicknesses (t_{CMG})=1.1 nm (4 ML), 0.57 nm (2 ML), and 0.29 nm (1 ML) were deposited on an Fe underlayer to stabilize the ferromagnetism of these ultrathin CMG films at RT and to prevent island growth of the thin films. Their sample-layer structures were as follows: (from the substrate side) MgO buffer layer (10 nm)/Fe underlayer (50 nm)/CMG thin film/MgO barrier (2 nm)/AlO_x(1 nm) capping layer, grown on a MgO(001) single-crystal substrate [type-1 layer structure, Fig. 1(a)]. Relatively thick CMG films with t_{CMG}=50 nm (172 ML), 2.9 nm (10 ML), and 1.7 nm (6 ML) were deposited on an MgO buffer layer. Their sample layer structures were as follows: (from the substrate side) MgO buffer layer (10 nm)/CMG thin film/MgO barrier (2 nm)/AlO_x (1 nm) capping layer [type-2 layer structure, Fig. 1(b)]. As a reference, we prepared a 4-ML-thick CMG film on the MgO buffer layer with type-1 layer structure. An ML of Co_2MnGe contains a Co plane and a Mn-Ge plane. A unit cell of CMG, which has a lattice parameter of 0.5743 nm, corresponds to 2 ML. Each sample layer was successively deposited in an ultrahigh vacuum chamber with a base pressure: about 6×10^{-8} Pa through the combined use of magnetron sputtering for Fe, CMG, and Al and electron beam evaporation for MgO. The Fe layer was deposited at RT on the MgO buffer layer, and subsequently annealed *in situ* at 400 °C. The CMG films were deposited at RT by rf magnetron sputtering from a stoichiometric Co_2MnGe target and those deposited on the Fe underlayer were subsequently annealed *in situ* at 325 °C for 15 min. To ensure that there was no Fe diffusion into the CMG film, we used a relatively low annealing temperature of 325 °C.[15,16] No signature of Fe diffusion was found for 325 °C annealing in the reflection high-energy electron-diffraction (RHEED) patterns observed *in situ* or in the comparison of the x-ray absorption spectroscopy (XAS)/XMCD evaluations of the 4-ML-thick CMG films with type-1 and type-2 structures. On the other hand, the CMG films deposited on the MgO buffer layer were subsequently annealed *in situ* at 500 °C for 15 min.[10,17] The pressure during the deposition of the MgO barrier was about 6×10^{-7} Pa. The AlO_x cap layer was prepared by exposing the sputter-deposited Al layer to an O_2 atmosphere ($\sim1\times10^{-5}$ Pa) for 2 h. We determined the sample-film composition by an inductively coupled plasma analysis with an accuracy of 2–3 % for each element. The CMG film composition was Co-rich (or both Mn- and Ge-deficient) $Co_2Mn_{0.77}Ge_{0.42}$.[10,17]

We observed 111 diffraction spots for a 50-nm-thick, Mn- and Ge-deficient CMG film deposited on an MgO buffer at RT and subsequently annealed *in situ* 500 °C by electron diffraction, indicating the $L2_1$ structure.[17] A cross-sectional high-resolution transmission electron microscope lattice image (HRTEM) showed that the identically prepared, Mn- and Ge-deficient 50-nm-thick CMG layer and the 2-nm-thick MgO barrier were grown epitaxially and were single crystalline.[17] The cross-sectional HRTEM image also confirmed that extremely smooth and abrupt interfaces were formed for the CMG/MgO barrier layer structure.[17] The epitaxial growth of all the layers with the (001) basal plane was confirmed for each successive layer in the MgO buffer/Fe underlayer/CMG/MgO structure and in the MgO buffer/CMG/MgO structure by *in situ* RHEED observations.

B. XMCD measurements

XMCD measurements were made by using circularly polarized soft x-rays on polarization-variable undulator beamline BL-16A and off-plane circularly polarized soft x-rays on bending magnet beamline BL-11A of the Photon Factory. The degree of circular polarization (P_c) was evaluated to be $P_c=\pm95\pm4\%$ on BL-16A, and $P_c=+87\pm4\%$ on BL-11A. The photon helicity (h) was fixed on BL-11A and reversed on BL-16A. The total-electron yield method was employed in the XAS and XMCD measurements. The angle between the incident x-rays and sample surface normal, θ, was changed by rotating the sample about the vertical axis but was usually set to 0°. XMCD measurements were also done at a "magic angle" of $\theta=54.7°$ ($3\cos^2\theta-1=0$), which allowed an accurate determination of the spin magnetic moment (m_{spin}).[18,19] Using a superconducting-magnet XMCD apparatus, magnetic fields of $B=\pm3$ T were applied to the sample parallel or antiparallel to h with $\theta=0°$ and 54.7°. All the measurements were made at RT.

III. EXPERIMENTAL RESULTS

A. Mn $L_{2,3}$-edge XMCD

Figure 2(a) shows the photon-flux-normalized polarization dependent XAS (μ_+ and μ_-) at the Mn $L_{2,3}$ ($2p_{1/2,3/2}\rightarrow3d$ absorption) edges. Figure 2(b) displays the Mn $L_{2,3}$-edge XMCD ($\Delta\mu=\mu_+-\mu_-$) spectra. Here, μ_+ and μ_- stand for the absorption coefficients for the photon helicity (h) parallel and antiparallel to the Mn $3d$ majority spin

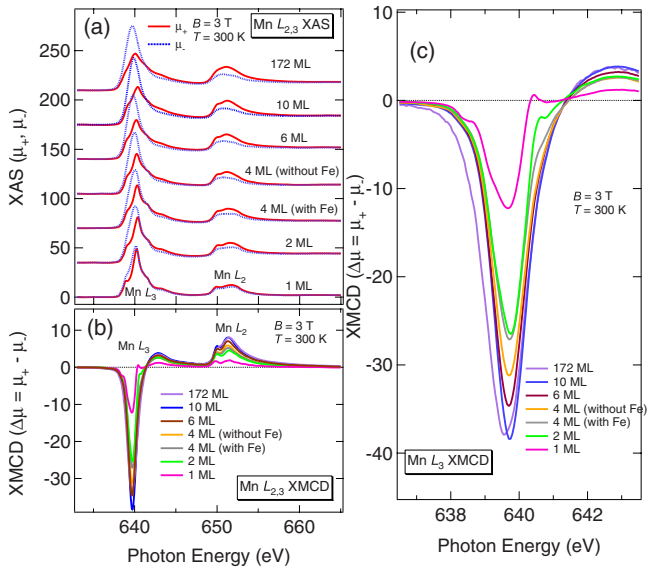

FIG. 2. (Color online) Normal-incidence (θ=0°) Mn $L_{2,3}$-edge XAS and XMCD of Co-rich CMG samples with various CMG thicknesses. (a) XAS measured at 300 K and $B=\pm 3$ T. μ_+ and μ_- are the absorption coefficients for the photon helicity parallel and antiparallel to the Mn 3d majority spin, respectively. (b) XMCD spectra given by $\Delta\mu=\mu_+-\mu_-$. (c) Magnified plots of XMCD spectra in Mn L_3-edge region.

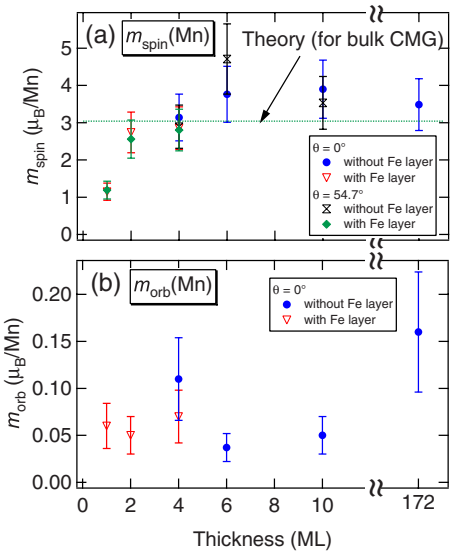

FIG. 3. (Color online) Film-thickness dependences of (a) Mn spin magnetic moment (m_{spin}) for θ=0° and 54.7° (magic angle) and (b) Mn orbital magnetic moment ($m_{orb}^{0°}$) for θ=0°. These were determined using the spin and orbital sum rules (Refs. 23 and 24). The theoretical spin-moment value for bulk CMG was taken from Ref. 27. The small difference between $m_{spin}^{0°}$ and $m_{spin}^{54.7°}$ represents the effect of the T_z term.

direction. A linear background has been subtracted from each XAS spectrum. In the XAS spectra for the 172-, 10-, 6-, and 4-ML samples, a shoulder was observed in the higher energy region of the Mn L_3 peak, and the Mn L_2 peak was split into a doublet. These features are characteristic of bulk CMG and CMS.[20] Because the probing depth of XAS and XMCD for $h\nu\sim 600-800$ eV is at most $\leq$5 nm, the XAS and XMCD spectra of the 172-ML sample reflect the bulk electronic structure in addition to the interfacial one of the CMG/MgO barrier (the upper side CMG/MgO interface). Except for the 172-ML sample, the XAS/XMCD spectra include signals from the lower side interface. However, signals from the lower side interface are reduced by $\exp(-t_{CMG}/\lambda)$ (~0.80, 0.71, and 0.56 for 4, 6, and 10 ML),[14] where $\lambda(\leq 5$ nm) is the probing depth of XAS and XMCD. Indeed, there was no detectable difference between the 172-ML sample and the other type-2 samples (4, 6, and 10 ML), indicating that contribution from the lower MgO/CMG interface was not significant even if it existed. The XMCD signal was reduced with decreasing t_{CMG}, in particular for t_{CMG}=2 and 1 ML [Fig. 2(b)]. In the Mn $L_{2,3}$-edge XAS for the 2- and 1-ML samples, a Mn^{2+}-like multiplet feature was observed, as in MnO (Refs. 21 and 22) [Fig. 2(a)]. Thus, the reduction of the ferromagnetic signal from the Mn atoms and the appearance of the multiplet feature in the XAS and XMCD spectra for the 1- and 2-ML samples indicate that the Mn atoms were oxidized in these ultrathin samples, which would be related to the possible deteriorated crystal structure of the ultrathin samples. In addition, the differences in XAS and XMCD between the 4-ML samples with and without Fe were small, although the XAS and XMCD spectra for the 4-ML samples include signals from the lower side MgO/CMG interface for the type-2 sample or from the lower-side Fe/CMG interface for the type-1 sample reduced by $\exp(-t_{CMG}/\lambda)$ (~0.80 for 4 ML) as mentioned above. Thus, the lower side interface does not significantly affect the electronic structure for $t_{CMG}>4$ ML.

Next, we determine m_{spin} and the orbital magnetic moment (m_{orb}) of the Mn atom by applying the sum rules[23,24] to the obtained XAS and XMCD spectra. The contribution of the intra-atomic magnetic dipole operator term T_z in the spin sum rule is negligibly small for thicker crystalline samples because the Mn site in CMG has T_d high symmetry. However, this assumption may not necessarily be valid for thinner samples because of their lowered symmetry. To accurately determine m_{spin}, we also measured Mn $L_{2,3}$-edge XAS and XMCD for the 1- to 10-ML samples at the magic angle of θ=54.7°, where the contribution of T_z vanishes.[18,19] Since there are overlapping regions of L_3 and L_2 due to strong exchange interaction between the Mn 2p core hole and the Mn 3d electrons in Mn^{2+} XAS and XMCD, we corrected the obtained m_{spin} by a factor 1/0.68, as given by Teramura *et al.*[25] We used the Mn 3d hole number of 4.5 (Ref. 26) which was taken from the band-structure calculations.[27] The results for θ=0° and =54.7° are shown in Fig. 3.

The spin magnetic moment for θ=0° deduced by neglecting the T_z term, $m_{spin}^{0°}$(Mn), was larger than 3 μ_B for t_{CMG} =6, 10, and 172 ML. $m_{spin}^{0°}$(Mn) dramatically decreased with decreasing t_{CMG} for $t_{CMG}<4$ ML, and $m_{spin}^{0°}$(Mn) for t_{CMG} =1 ML was as small as 1.15 μ_B, while $m_{spin}^{0°}$(Mn) for the bulklike 172- and 10-ML samples was larger than the theoretical value of 3.04 μ_B.[27] The spin moment for the magic angle of θ=54.7° without any contribution from T_z, $m_{spin}^{54.7°}$(Mn), is also shown as a function of t_{CMG} in Fig. 3(a). The values for each thickness are summarized in Table I. The

TABLE I. Spin and orbital magnetic moments of Mn and Co atoms deduced from sum-rule analyses of XMCD spectra.

	1 ML	2 ML	4 ML	4 ML	6 ML	10 ML	172 ML
	With Fe			Without Fe			
$m_{\mathrm{spin}}^{0^\circ}$(Mn) ($\mu_B$)	1.15	2.74	2.85	3.14	3.76	3.90	3.49
$m_{\mathrm{orb}}^{0^\circ}$(Mn) ($\mu_B$)	0.06	0.05	0.07	0.11	0.04	0.05	0.16
$m_{\mathrm{spin}}^{54.7^\circ}$(Mn) ($\mu_B$)	1.19	2.56	2.80	2.89	4.71	3.53	
$m_{\mathrm{spin}}^{0^\circ}$(Co) ($\mu_B$)	1.77	1.46	1.26	1.47	1.27	1.38	1.40
$m_{\mathrm{orb}}^{0^\circ}$(Co) ($\mu_B$)	0.14	0.06	0.16	0.13	0.13	0.09	0.16
$m_{\mathrm{spin}}^{54.7^\circ}$(Co) ($\mu_B$)	1.58	1.61	1.21	1.40	1.49	1.30	

difference between $m_{\mathrm{spin}}^{0^\circ}$(Mn) and $m_{\mathrm{spin}}^{54.7^\circ}$(Mn), i.e., the T_z term, is small even for the thin samples. The considerably reduced $m_{\mathrm{spin}}^{0^\circ}$(Mn) and $m_{\mathrm{spin}}^{54.7^\circ}$(Mn) for the 1-ML sample indicate that the Mn atoms were oxidized. The orbital magnetic moment for $\theta=0^\circ$, $m_{\mathrm{orb}}^{0^\circ}$(Mn), was found to be 0.05–0.10 μ_B for all the samples [Fig. 3(b) and Table I], that is, $m_{\mathrm{orb}}^{0^\circ}$(Mn) did not show any clear film-thickness dependence. For all the samples, m_{spin}(Mn) and m_{orb}(Mn) had the same sign, indicating that the Mn 3*d* state was more than half filled, with an electron occupation number of $n_{3d}(\mathrm{Mn})>5$, which was consistent with the theoretical Mn 3*d* hole number of $n_h(\mathrm{Mn})=4.5$ (Ref. 26) used for the sum rules.

Saito *et al.*[28] reported CMS-film-thickness-dependent XMCD and theoretical studies on slightly Co-rich $Co_2Mn_{0.91}Si_{0.93}$/MgO also grown on an Fe underlayer. Their experimental m_{spin}(Mn) in CMS increased with decreasing CMS thickness, except for a 1-ML sample, and the theoretical m_{spin}(Mn) in the case of Mn-Si termination was consistent with their XMCD results. The m_{spin}(Mn) of CMS was reduced only for the 1-ML sample but the XAS and XMCD spectra for the 1-ML sample did not show any Mn^{2+}-like multiplet structure indicating the absence of oxidation.[28] On the other hand, the present experimental results on the Co-rich CMG/MgO showed reduced m_{spin}(Mn) due to the oxidation of Mn atoms in the 1- and 2-ML samples. The quality of the crystal structure of the ultrathin Co-rich CMG samples should not be as good as that of the slightly Co-rich 1-ML CMS. The structural difference would be related to the different oxidation tendencies.

B. Co $L_{2,3}$-edge XMCD

Figure 4(a) shows the photon flux-normalized, polarization-dependent XAS at the Co $L_{2,3}$ edges. Figure 4(b) displays the Co $L_{2,3}$-edge XMCD spectra. For all the samples, a shoulder, which is common to bulk samples,[20] was observed in the higher energy region of the Co L_3-edge XAS. The XMCD signals increased as the film thickness decreased, implying that the Co atoms in the ultrathin samples were strongly spin polarized. No CoO-like multiplet structure[29] was found in any of the samples, indicating that the Co atoms were not oxidized even in the ultrathin samples. In addition, the differences in XAS and XMCD between the 4-ML samples with and without Fe were not so large.

We determined the Co magnetic moments by using the sum rules[23,24] similarly to the Mn $L_{2,3}$ edges. While the Co atoms in the thicker samples are in the highly symmetric T_d crystal field, we measured Co $L_{2,3}$-edge XAS and XMCD at the magic angle of $\theta=54.7^\circ$ in order to accurately determine the spin moment. We used a theoretical Co 3*d* hole number of 2.2 (Ref. 26) in applying the sum rules. The results are shown in Fig. 5.

The Co spin moment for $\theta=0^\circ$ obtained by neglecting the T_z term, $m_{\mathrm{spin}}^{0^\circ}$(Co), was 1.40 μ_B for the 172-ML sample and was enhanced to 1.77 μ_B for the 1-ML sample while $m_{\mathrm{spin}}^{0^\circ}$(Co) was around 1.40 μ_B for $t_{\mathrm{CMG}}\geq 2$ ML. For all the samples, $m_{\mathrm{spin}}^{0^\circ}$(Co) was larger than the theoretical value of 0.98 μ_B.[27] The spin moment for the magic angle of $\theta=54.7^\circ$ without any contribution from T_z, $m_{\mathrm{spin}}^{54.7^\circ}$(Co), is also shown as a function of t_{CMG} in Fig. 5. The magnetic-moment values for each thickness are summarized in Table I. The difference between $m_{\mathrm{spin}}^{0^\circ}$(Co) and $m_{\mathrm{spin}}^{54.7^\circ}$(Co) was small,

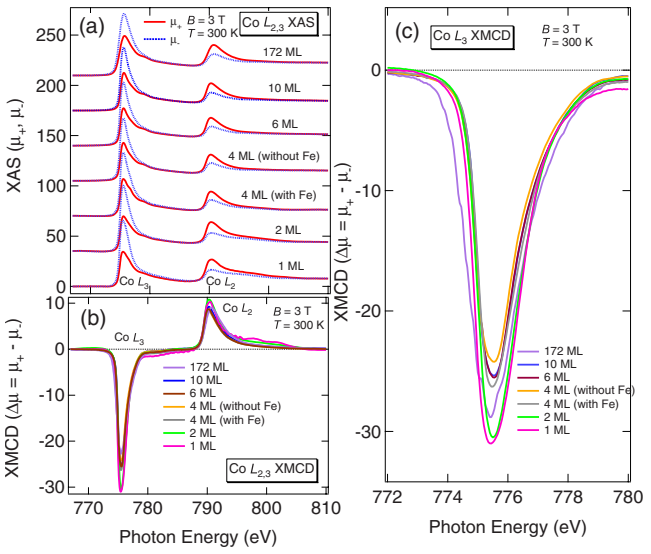

FIG. 4. (Color online) Normal-incidence ($\theta=0^\circ$) Co $L_{2,3}$-edge XAS and XMCD of Co-rich Co_2MnGe samples with various CMG thicknesses. (a) XAS measured at 300 K and $B=\pm 3$ T. μ_+ and μ_- are the absorption coefficients for photon helicity parallel and antiparallel to the Co 3*d* majority spin, respectively. (b) XMCD spectra given by $\Delta\mu=\mu_+-\mu_-$. (c) Magnified plots of XMCD spectra in Co L_3-edge region.

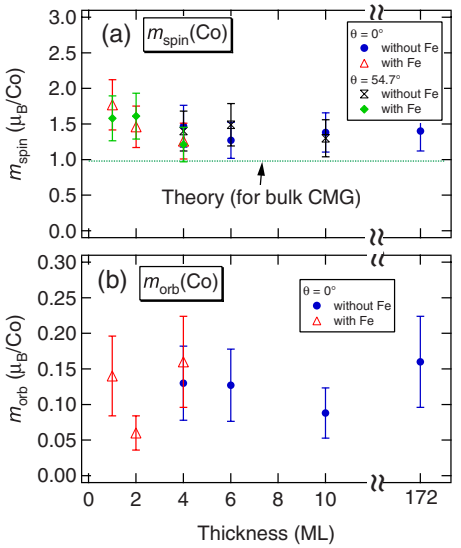

FIG. 5. (Color online) Film-thickness dependences of (a) Co spin magnetic moment (m_{spin}) for θ=0° and 54.7° (magic angle) and (b) Co orbital magnetic moment ($m_{orb}^{0°}$) for θ=0°. These were determined using the spin and orbital sum rules (Refs. 23 and 24). The theoretical spin-moment value for bulk CMG was taken from Ref. 27. The small difference between $m_{spin}^{0°}$ and $m_{spin}^{54.7°}$ represents the effect of the T_z term.

showing that the effect of the T_z term was small. The tendency for the spin moment of Co to increase for the thinner samples was common for θ=0° and 54.7°. The orbital moment for θ=0°, $m_{orb}^{0°}$(Co), was about 0.10 μ_B for all the samples. The CMS film-thickness-dependent XMCD studies and first principles calculations by Saito *et al.*[28] revealed that the m_{spin}(Co) of CMS was enhanced for CMS thicknesses (t_{CMS})<4 ML. This enhancement was explained by an Fe/Co interfacial effect at the lower side interface. They reported that the MnSi termination with MnO bond at the upper side interface was energetically stable regardless of t_{CMS}.[28] As a consequence, the lower side Fe/Co interface was also favored for t_{CMS}=1 ML. Since the layer structure of the CMS/MgO heterostructures[28] was quite similar to that of the present CMG/MgO heterostructures, the enhanced m_{spin}(Co) for the CMG/MgO ultrathin samples could also be due to the Fe/Co interfacial effect at the lower side interface.

IV. DISCUSSION

We discuss the oxidation of the Mn in the nonstoichiometric CMG ultrathin films facing an MgO barrier. Saito *et al.*[16] reported in their XMCD study on CMS/MgO that the m_{spin}(Mn) of intentionally oxidized CMS was almost zero and Mn $L_{2,3}$-edge XAS clearly showed an MnO-like Mn^{2+} multiplet structure. In contrast, the Co $L_{2,3}$-edge XAS of intentionally oxidized CMS showed no multiplet structure, and the Co $L_{2,3}$-edge XMCD was similar to that of unoxidized CMS. They concluded that, in CMS, Mn atoms were easily oxidized compared with Co atoms, which is consistent with our result that the Co atoms, even in the 1- and 2-ML samples, were highly stable against oxidation compared with the Mn atoms.

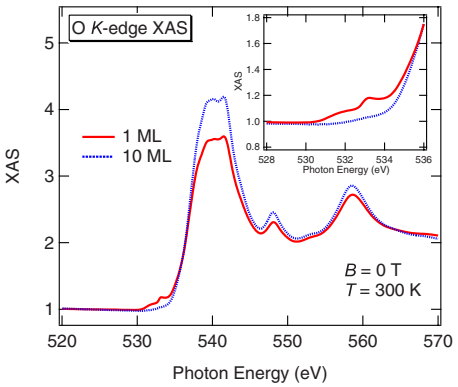

FIG. 6. (Color online) O *K*-edge XAS for 1- and 10-ML samples. The inset shows a magnified plot of the pre-edge region. The two XAS have been normalized in intensity to unity at around 520–530 eV.

Figure 6 shows the O *K*-edge XAS spectra (B=0 T) of the 1- and 10-ML samples. The strong peaks observed for $h\nu$>535 eV originate from oxygen in the MgO barrier[30] and AlO_x capping layer. Interestingly, pre-edge structures were clearly observed for the 1-ML sample at 530 eV<$h\nu$<535 eV. It is known that neither MgO nor AlO_x exhibit such pre-edge features but MnO does show them[21,31] in O *K*-edge XAS, in sharp contrast to the main peaks for $h\nu$>535 eV. Thus, these features could be attributed uniquely to MnO formed at the interfaces. The existence of the pre-edge structures for the 1-ML sample also supports again our view of oxidized Mn atoms.

Sicot *et al.*[32] reported x-ray photoemission, XAS, and XMCD studies of Co, Fe, and Mn metals facing MgO. They revealed that Co and Fe metals were not oxidized after MgO growth on them but that Mn metal was oxidized, particularly at the interfacial region, which is consistent with the present results for the 1- and 2-ML samples. Furthermore, the enthalpy of formation of MnO(−92 kcal/mol) is lower than that of CoO(−57 kcal/mol).[33] Saito *et al.*[28] reported that the calculated m_{spin}(Mn) and m_{spin}(Co) for CMS/MgO in the case of MnSi termination (MnSi/MgO interface) with Mn-O bonds well explained their experimental results in contrast to the case of Co termination (Co/MgO interface). In this context, for the present 1-ML CMG sample, a MnGe termination, i.e., a layer structure of (Fe underlayer)/(Co layer)/(MnGe layer)/MgO with Mn-O bonds, should be energetically more stable. We therefore conclude that the interfacial Mn atoms in the ultrathin CMG samples were easily oxidized while the Co atoms were highly stable against oxidation. Comparing m_{total}(Mn)=m_{spin}(Mn)+m_{orb}(Mn) for the 1-ML sample with m_{total}(Mn) for the 10-ML sample, we estimated that about 70% of the Mn atoms in the 1-ML sample were oxidized. Here, we assumed that all the Mn atoms in the 10-ML sample were not oxidized.

To confirm the validity of our estimation, we subtracted 30% of the Mn $L_{2,3}$-edge XAS for the 10-ML sample, which would correspond to the contribution of the unoxidized Mn in the 1-ML sample as discussed above, from that for the 1-ML one. The result is shown in Fig. 7. The subtraction-deduced spectrum is very similar to the Mn $L_{2,3}$-edge XAS

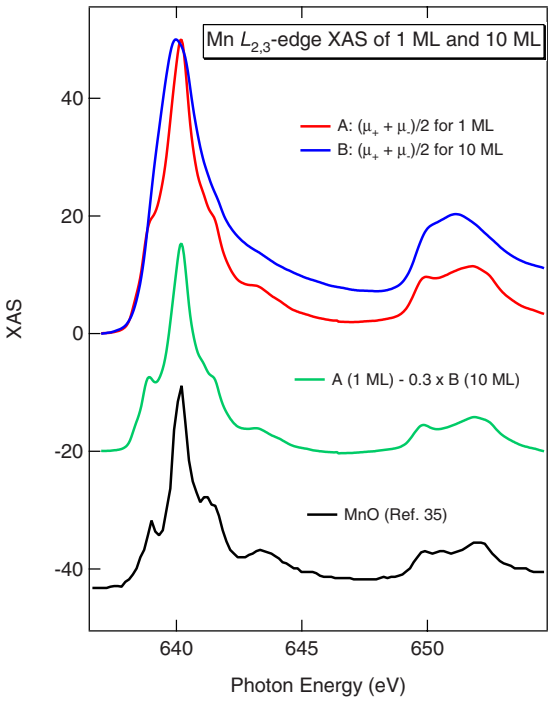

FIG. 7. (Color online) Comparison of Mn $L_{2,3}$-edge XAS for 1-ML sample and that of 10-ML one (top two curves). The middle green spectrum is obtained by the subtraction (1 ML)−0.3 ×(10 ML). The bottom black spectrum is the Mn $L_{2,3}$-edge XAS of MnO taken from Ref. 35.

of MnO.[21,34–36] Because MnO is a paramagnetic insulator at RT and an antiferromagnetic insulator below $T_N \sim 120$ K,[37] a large number (~70%) of oxidized Mn atoms in the 1-ML sample did not contribute to the ferromagnetism.

Here, we discuss possible origins of the observed oxidation of Mn in the ultrathin 1- and 2-ML samples. The observed oxidation of Mn in the ultrathin CMG/MgO samples is in contrast to the absence of that in the CMS/MgO samples. It should be noted that the present CMG film composition was Mn-deficient and highly Ge-deficient ($Co_2Mn_{0.77}Ge_{0.42}$), in contrast to the slightly Mn- and Si-deficient film composition of the CMS film ($Co_2Mn_{0.91}Si_{0.93}$) in the CMS/MgO samples.[28] In accordance with the chemical composition model for Mn- and Ge-deficient CMG films[38] developed by taking into consideration the formation energies of various kinds of defects,[39] the chemical composition for nonstoichiometric $Co_2Mn_{0.77}Ge_{0.42}$ film is estimated to be $Co_2[Mn_{0.49}Co_{0.51}][Ge_{0.53}Mn_{0.47}]$, where $[Mn_{0.49}Co_{0.51}]$ and $[Ge_{0.53}Mn_{0.47}]$ represent the nominal Mn and Ge sites, respectively. Similarly, the chemical composition for the slightly Mn- and Si-deficient CMS film of $Co_2Mn_{0.91}Si_{0.93}$ is estimated to be $Co_2[Mn_{0.92}Co_{0.08}][Si_{0.97}Mn_{0.03}]$. Thus, the degrees of order of the nominal Mn and Ge sites in $Co_2Mn_{0.77}Ge_{0.42}$ films should be significantly lower than those in the nominal Mn and Si sites in $Co_2Mn_{0.91}Si_{0.93}$. Furthermore, the degree of structural order would be lower for ultrathin CMG (CMS) films with 1- and 2-ML thicknesses, resulting in increased disorder between the nominal Mn-Ge (Mn-Si) plane and the nominal Co plane. The decreased degree of structural order in the ultrathin CMG films along with the highly disordered nominal Mn and Ge sites would be a possible reason of the observed oxidation of Mn in the 1- and 2-ML samples.

Next, we discuss the effects of antisites defects in the nonstoichiometric CMG/MgO thin films. The deduced m_{spin}(Co) for all the CMG samples was obviously larger than a theoretical value of ~1 μ_B (Ref. 27) and the experimental XMCD value of 1.04 μ_B for the bulk samples reported by Miyamoto *et al.*[40,41] Note that their XMCD study was done at $B=1.4$ T and $T=45$ K and that they scraped the bulk CMG samples to obtain clean surfaces and used a Co 3*d* hole number of 3.0.[40,41] Picozzi *et al.*[42] investigated theoretically the effect of antisite defects in CMG and CMS. They reported that m_{spin}(Co) of the Co antisites in CMG, Co_{Mn}, was 1.35 μ_B, which was larger than 1.06 μ_B for Co at the regular Co site, Co_{Co}. Here, the Co antisites mean Co atoms occupying Mn sites in regular CMG. The present large m_{spin}(Co) of 1.40–1.77 μ_B therefore indicates the possibility of the existence of Co_{Mn}. We confirmed by *in situ* RHEED that the present CMG samples on which we measured XMCD had the disorder-free $L2_1$ structure. However, since the film composition was Co:Mn:Ge=2:0.77:0.42 deviating from 2: 1: 1, some Co atoms possibly occupy the Mn site. The calculated total DOS for each of the majority- and minority-spin bands of CMG was reported,[42] and in-gap states were found to exist within the minority-spin gap only when Co_{Mn} existed. The possible existence of Co_{Mn} in CMG may lead to a decrease in the spin polarization. This consideration is consistent with that the spin polarization of Co-rich CMG estimated from the TMR ratio at 4.2 K for CMG/MgO/CoFe MTJs assuming Jullière's model, P_{CMG}, was as low as 0.74.[6]

It was reported that the m_{spin}(Co) of Co-rich CMS/MgO was 1.16 μ_B for a sample with $t_{CMS}=50$ nm, and 1.25 μ_B for a sample with $t_{CMS}=1.1$ nm (4 ML),[43] both being larger than a theoretical value of 1.06 μ_B.[27] The CMS film composition of Co:Mn:Si=2:0.91:0.93 was Co-rich similar to the Co-rich CMG that we have studied here. Consequently, the Co-rich CMS might have had more or less the same amount of Co_{Mn} as in Co-rich CMG. Picozzi *et al.*[42] reported that in-gap states could theoretically exist within the minority-spin gap for CMS with Co_{Mn}. The spin polarization of Co-rich CMS estimated from the TMR ratio at 4.2 K for CMS/MgO/CoFe MTJs assuming Jullière's model, P_{CMS}, was as low as 0.75.[7] The comparison between Co-rich CMG and Co-rich CMS can be summarized as follows: (i) the deviation in composition from 2:1:1 for CMG is larger than that for CMS, (ii) the P_{CMG} of 0.74 (Ref. 6) is comparable to the P_{CMS} of 0.75,[7] and (iii) the difference in m_{spin}(Co) between the present XMCD results and the theories for CMG is larger than that for CMS.[27]

The spin polarization at E_F and the spin moment would be influenced by nonstoichiometry in CMG thin films. To reduce the minority-spin in-gap DOS and to improve the TMR ratio, appropriate control of the film composition is critical.[38,44] A promising method is to prepare CMG films by cosputtering from CMG, Mn, and Ge targets to appropriately control the CMG film composition. In fact, high TMR ratios of 650% at 4.2 K and 220% at RT have been demonstrated for CMG/MgO/CMG MTJs with Mn-rich $Co_2Mn_{1.40}Ge_{0.38}$

electrodes prepared by cosputtering from CMG and Mn targets.[38] In addition, theoretical studies have revealed that Mn antisites (located at the regular Co sites) in Mn-rich CMS do not affect the half-metallic gap.[39]

V. CONCLUSION

We studied the magnetic and electronic states of Co_2MnGe/MgO magnetic tunnel junctions by CMG film-thickness dependent XMCD measurements. The XAS and XMCD spectral shapes for thick samples ($t_{CMG} \geq 4$ ML) were similar to those for bulk CMG,[20,40,41] and neither the Mn nor Co atoms were oxidized. We have found that about 70% of the Mn atoms in the 1-ML sample were oxidized. The lattice distortions and disorder in the ultrathin samples would be related to oxidation. In contrast, Co atoms in the ultrathin samples were not oxidized and more strongly spin polarized. The enhanced m_{spin}(Co) for the ultrathin samples could be due to the Fe/Co interfacial effect as in CMS/MgO heterostructures.[28] The existence of Co antisites is suggested by considering theories on Co antisites[27,42] and the observed m_{spin}(Co) of 1.40–1.77 μ_B, which was larger than theoretical values for ideal compounds.

The nonstoichiometry of the Co-rich CMG samples is also consistent with the existence of Co antisites. In-gap states have been predicted to exist within the Co minority-spin band gap when Co antisites are present.[42] The consideration is consistent with the experimental results that the TMR ratios at both 4.2 K and RT of CMG/MgO/CMG MTJs with Co-rich CMG electrodes were considerably lower than those of CMG/MgO/CMG MTJs with Mn-rich CMG electrodes.[38] CMG-composition and temperature-dependent XMCD studies would be desirable in the near future to fully understand the electronic states of CMG with an MgO barrier. Spin-resolved photoemission studies would also be desirable to directly observe the half-metallic nature of Heusler alloys.

ACKNOWLEDGMENTS

This work was carried out with the approval of the Photon Factory Program Advisory Committee (Proposals No. 2006G235 and No. 2008G121). This work was supported by Grants-in-Aid for Scientific Research in the Priority Area "Creation and Control of Spin Current" (Grants No. 19048012 and No. 19048001) from the Ministry of Education, Culture, Sports, Science and Technology, Japan, and the "Quantum Beam Technology Development Program" of the Japan Science and Technology Agency.

[1] S. Yuasa, T. Nagahama, A. Fukushima, Y. Suzuki, and K. Ando, Nature Mater. **3**, 868 (2004).
[2] S. Ishida, S. Fujii, S. Kashiwagi, and S. Asano, J. Phys. Soc. Jpn. **64**, 2152 (1995).
[3] R. A. de Groot, F. M. Mueller, P. G. van Engen, and K. H. J. Buschow, Phys. Rev. Lett. **50**, 2024 (1983).
[4] M. I. Katsnelson, V. Yu. Irkhin, L. Choicel, A. I. Lichtenstein, and R. A. de Groot, Rev. Mod. Phys. **80**, 315 (2008).
[5] S. Picozzi, A. Continenza, and A. J. Freeman, Phys. Rev. B **66**, 094421 (2002).
[6] S. Hakamata, T. Ishikawa, T. Marukame, K.-i. Matsuda, T. Uemura, M. Arita, and M. Yamamoto, J. Appl. Phys. **101**, 09J513 (2007).
[7] T. Ishikawa, T. Marukame, H. Kijima, K.-i. Matsuda, T. Uemura, M. Arita, and M. Yamamoto, Appl. Phys. Lett. **89**, 192505 (2006).
[8] T. Marukame, T. Ishikawa, S. Hakamata, K.-i. Matsuda, T. Uemura, and M. Yamamoto, Appl. Phys. Lett. **90**, 012508 (2007).
[9] T. Taira, T. Ishikawa, N. Itabashi, K.-i. Matsuda, T. Uemura, and M. Yamamoto, Appl. Phys. Lett. **94**, 072510 (2009).
[10] T. Marukame, T. Ishikawa, K.-i. Matsuda, T. Uemura, and M. Yamamoto, J. Appl. Phys. **99**, 08A904 (2006).
[11] T. Miyazaki and N. Tezuka, J. Magn. Magn. Mater. **151**, 403 (1995).
[12] M. Jullière, Phys. Lett. A **54**, 225 (1975).
[13] M. J. Carey, T. Block, and B. A. Gumey, Appl. Phys. Lett. **85**, 4442 (2004).
[14] R. Nakajima, J. Stöhr, and Y. U. Idzerda, Phys. Rev. B **59**, 6421 (1999).
[15] S. Yuasa, T. Katayama, T. Nagahama, A. Fukushima, H. Kubota, Y. Suzuki, and K. Ando, Appl. Phys. Lett. **87**, 222508 (2005).
[16] T. Saito, T. Katayama, T. Ishikawa, M. Yamamoto, D. Asakura, and T. Koide, Appl. Phys. Lett. **91**, 262502 (2007).
[17] T. Taira, T. Ishikawa, N. Itabashi, K.-i. Matsuda, T. Uemura, and M. Yamamoto, J. Phys. D **42**, 084015 (2009).
[18] J. Stöhr and H. König, Phys. Rev. Lett. **75**, 3748 (1995).
[19] T. Koide, H. Miyauchi, J. Okamoto, T. Shidara, A. Fujimori, H. Fukutani, K. Amemiya, H. Takeshita, S. Yuasa, T. Katayama, and Y. Suzuki, Phys. Rev. Lett. **87**, 257201 (2001).
[20] K. Miyamoto, K. Iori, A. Kimura, T. Xie, M. Taniguchi, S. Qiao, and K. Tsuchiya, Solid State Commun. **128**, 163 (2003).
[21] V. Bayer, R. Podloucky, C. Franchini, F. Allegretti, B. Xu, G. Parteder, M. G. Ramsey, S. Surnev, and F. P. Netzer, Phys. Rev. B **76**, 165428 (2007).
[22] B. T. Thole, R. D. Cowan, G. A. Sawatzky, J. Fink, and J. C. Fuggle, Phys. Rev. B **31**, 6856 (1985).
[23] B. T. Thole, P. Carra, F. Sette, and G. van der Laan, Phys. Rev. Lett. **68**, 1943 (1992).
[24] P. Carra, B. T. Thole, M. Altarelli, and X. Wang, Phys. Rev. Lett. **70**, 694 (1993).
[25] Y. Teramura, A. Tanaka, and T. Jo, J. Phys. Soc. Jpn. **65**, 1053 (1996).
[26] J. Grabis, A. Bergmann, A. Nefedov, K. Westerholt, and H. Zabel, Phys. Rev. B **72**, 024437 (2005).
[27] I. Galanakis, P. H. Dederichs, and N. Papanikolaou, Phys. Rev. B **66**, 174429 (2002).
[28] T. Saito, T. Katayama, T. Ishikawa, M. Yamamoto, D. Asakura, T. Koide, Y. Miura, and M. Shirai, Phys. Rev. B **81**, 144417 (2010).
[29] T. J. Regan, H. Ohldag, C. Stamm, F. Nolting, J. Lüning, J.

Stöhr, and R. L. White, Phys. Rev. B **64**, 214422 (2001).
[30] S. I. Nakai, T. Mitsuishi, H. Sugawara, H. Maezawa, T. Matsukawa, S. Mitani, K. Yamasaki, and T. Fujikawa, Phys. Rev. B **36**, 9241 (1987).
[31] E. Z. Kurmaev, R. G. Wilks, A. Moewes, L. D. Finkelstein, S. N. Shamin, and J. Kuneŝ, Phys. Rev. B **77**, 165127 (2008).
[32] M. Sicot, S. Andrieu, F. Bertran, and F. Fortuna, Phys. Rev. B **72**, 144414 (2005).
[33] *Lange's Handbook of Chemistry*, 13th ed., edited by J. Dean (McGraw-Hill, New York, 1985).
[34] M. Kohgi, Y. Ishikawa, I. Harada, and K. Motizuki, J. Phys. Soc. Jpn. **36**, 112 (1974).
[35] F. M. F. de Groot, J. Electron Spectrosc. Relat. Phenom. **67**, 529 (1994).
[36] H. J. Lee, G. Kim, D. H. Kim, J.-S. Kang, C.-L. Zhang, S.-W. Cheong, J.-H. Shim, S. Lee, H. Lee, J.-Y. Kim, B.-H. Kim, and B. I. Min, J. Phys.: Condens. Matter **20**, 295203 (2008).
[37] B. Gilbert, B. H. Frazer, A. Belz, P. G. Conrad, K. H. Nelson, D. Haskel, J. C. Lang, G. Srajer, and G. De Stasio, J. Phys. Chem. A **107**, 2839 (2003).
[38] M. Yamamoto, T. Ishikawa, T. Taira, G.-F. Li, K.-i. Matsuda, and T. Uemura, J. Phys.: Condens. Matter **22**, 164212 (2010).
[39] B. Hülsen, M. Scheffler, and P. Kratzer, Phys. Rev. B **79**, 094407 (2009).
[40] K. Miyamoto, A. Kimura, K. Iori, T. Xie, K. Sakamoto, T. Moko, S. Qiao, M. Taniguchi, and K. Tsuchiya, Physica B **351**, 347 (2004).
[41] K. Miyamoto, A. Kimura, K. Iori, K. Sakamoto, T. Xie, T. Moko, S. Qiao, M. Taniguchi, and K. Tsuchiya, J. Phys.: Condens. Matter **16**, S5797 (2004).
[42] S. Picozzi, A. Continenza, and A. J. Freeman, Phys. Rev. B **69**, 094423 (2004).
[43] T. Saito, T. Katayama, A. Emura, N. Sumida, N. Matsuoka, T. Ishikawa, T. Uemura, M. Yamamoto, D. Asakura, and T. Koide, J. Appl. Phys. **103**, 07D712 (2008).
[44] T. Ishikawa, H.-x. Liu, T. Taira, K.-i. Matsuda, T. Uemura, and M. Yamamoto, Appl. Phys. Lett. **95**, 232512 (2009).